Journal of Alloys and Compounds 509 (2011) 7162–7167

Contents lists available at ScienceDirect

Journal of Alloys and Compounds

journal homepage: www.elsevier.com/locate/jallcom

Effects of cyclic hydriding–dehydriding reactions of Mg_2Ni alloy on the expansion deformation of a metal hydride storage vessel

Chih-Kuang Lin*, Sih-Ming Huang, Yu-Hao Jhang

Department of Mechanical Engineering, National Central University, 300 Jhong-Da Rd., Jhong-Li 32001, Taiwan

ARTICLE INFO

Article history:
Received 21 January 2011
Received in revised form 1 April 2011
Accepted 5 April 2011
Available online 12 April 2011

Keywords:
Mg_2Ni
Hydriding–dehydriding reaction
Metal hydride storage vessel
Expansion deformation

ABSTRACT

A high-temperature reaction vessel system was set up to study the wall deformation during cyclic hydriding/dehydriding reactions of Mg_2Ni powders at 255 °C. Effects of packing fraction and initial particle size of Mg_2Ni powders were characterized. Results indicated that a strain accumulation was found on the wall surface with progressive cycles of hydriding/dehydriding reactions. The wall strain varied with position, as a lower position had a larger deformation. Such an accumulation and position-dependence of wall strain in the vertical hydride storage vessel could be attributed to a pulverization-densification mechanism. At a given vessel position, the hoop strain was increased with increasing packing fraction from 50 to 70 vol%. For a 50-vol% packing fraction, the wall deformation was enlarged when the initial powder size was increased from 200 mesh (74 μm) to 100 mesh (149 μm). After 50 cycles of hydriding/dehydriding reactions, the particle size was significantly reduced to about 1 μm.

1. Introduction

Magnesium is considered a promising medium for hydrogen storage due to its high hydrogen storage capacity and low cost, as compared to other metals [1,2]. Magnesium hydride, MgH_2, can absorb as high as 7.6 wt% of hydrogen [3]. However, there are certain limitations of pure magnesium for use as a hydrogen storage medium, including susceptibility to oxidation, slow hydriding/dehydriding kinetics, and high temperature of hydrogen desorption [1,2]. Therefore, a pure magnesium is usually alloyed with other elements to overcome some of the disadvantages to certain extents. Among the alloys developed in this regard, Mg_2Ni is the most popular alloy which can reduce the dehydrogenation temperature [4,5]. In addition, nickel also can facilitate the dissociation of molecular hydrogen on the surface of the hydrogen storage media to improve the kinetics of a hydriding/dehydriding process [6]. The hydrogen storage capacity of the hydride of Mg_2Ni, Mg_2NiH_4, is about 3.6 wt%, which is better than that of other types of non-Mg-based metal hydrides [2,3]. Mg_2Ni and its modified alloys have been getting more attention to be used as an on-board hydrogen storage medium or negative electrode in Ni-MH batteries [1,2,7–9]. Previous efforts to decrease the desorption temperature and enhance the kinetics and cyclic life for Mg_2Ni-type alloys have been systematically summarized and discussed in two recent reviews [1,2]. A few more attempts have recently been made to improve the hydrogen storage characteristics of Mg_2Ni-type alloys, e.g. through techniques involving melt spinning, rapid quenching, wet ball milling, and alloying with other elements [7–10]. Although Mg_2Ni usually has to absorb/desorb hydrogen at temperature higher than 200 °C, the plateau slope and cyclic stability characteristics expressed in the pressure–composition–isotherm (PCI) curves of Mg_2Ni are good for practical applications [11,12]. Therefore, Mg_2Ni is a favorable hydrogen storage candidate for vehicular application due to its high gravimetric hydrogen storage capacity, low cost, and low-toxicity [1,2]. Mg_2Ni is thus chosen as the hydrogen storage material investigated in the current study.

For metal hydrides to be used in many applications, they need to be filled into a reactor, so called hydride storage vessel, in which hydriding and dehydriding reactions take place. A proper design of hydride storage vessel is important to ensure a good performance for a selected hydrogen storage alloy. There are several issues needed to be considered in design of a hydride storage vessel scheme, such as primary configuration, thermal management, hydrogen transfer, and mechanistic strength [13]. Many numerical and experimental studies have been focused on the coupling process of porous flow, heat and mass transfer, and reaction kinetics to find the optimal design and operation parameters for variously designed hydride storage vessels, e.g. in [13–20]. Some techniques have recently been proposed to improve the performance of hydride storage vessels, e.g. by using an internal spiral heat exchanger with fins [21,22] or concentric heat exchanger with fins [22,23], an internal metal foam [24], and cylindrical pellets of hydride [25]. Up to date, only a few studies have investigated the mechanistic strength and structural deformation of hydride

* Corresponding author. Tel.: +886 3 426 7340; fax: +886 3 425 4501.
E-mail address: t330014@cc.ncu.edu.tw (C.-K. Lin).

0925-8388/$ – see front matter © 2011 Elsevier B.V. All rights reserved.
doi:10.1016/j.jallcom.2011.04.038

storage vessels [26–33]. When a metallic alloy absorbs hydrogen, its volume will expand. For example, the volume expansion ratio during hydrogen absorption is 24% for $LaNi_5$ [31] and 28–32% for Mg_2Ni [34,35]. Such a volume expansion could induce wall stress and deformation in the storage vessel. For an improper vessel design, a large change in the specific volume of a metal hydride during hydriding/dehydriding cycles might result in permanent deformation and/or cracking on the vessel wall. Therefore, it is important to study the expansion characteristics of metal hydrides and their influences on the wall deformation for design of a reliable hydride storage vessel. Previous studies on these issues were almost focused on $LaNi_5$ and its multiphase alloys [26–32] which can absorb and desorb hydrogen at room temperature. As described above, Mg_2Ni has a greater hydrogen storage capacity than $LaNi_5$ and is potentially to be used for vehicular application. In addition, the volume expansion ratio of Mg_2Ni during hydrogen absorption is larger than that of $LaNi_5$ and the hydriding/dehydriding reactions of Mg_2Ni work at temperature above 200 °C instead at room temperature [1]. However, it is difficult to measure wall strain variation in the storage vessel of Mg_2Ni at 200–350 °C which has never been studied before. If the wall expansion strain induced by formation of Mg_2NiH_4 is characterized, it will be helpful to assess the structural reliability of a high-temperature Mg_2Ni storage vessel. Therefore, the aim of this study is to investigate the expansion deformation of a high-temperature storage vessel under cyclic hydriding/dehydriding reactions of Mg_2Ni alloy. In particular, the influences of packing fraction and initial particle size of Mg_2Ni powders on the wall strain variation are characterized for a given storage vessel at 255 °C. It is hoped that the characteristics of wall deformation induced by Mg_2NiH_4 formation presented in the current study is helpful for design and future applications of high-temperature Mg_2Ni storage vessels.

2. Experimental procedures

2.1. Experimental setup

Fig. 1 shows the geometry and dimensions of a thin-wall hydride storage vessel designed and made in house. The wall thickness of the cylindrical vessel is 1 mm. The inner diameter and height of the free space in the given vessel is 20 and 64 mm, respectively. The vessel is made of an AISI 316 stainless steel. Wall strain measurements during cyclic hydriding/dehydriding reactions were performed using the experimental setup shown in Fig. 2. SV1-SV8 are the solenoid valves used to control the hydrogen flow route. P1–P3 are the pressure transducers used to monitor the extracting hydrogen pressure, input hydrogen pressure, and hydrogen pressure in the vessel, respectively. A 0.5-μm-grade tubular filter is attached at the top flange of the vessel to prevent Mg_2Ni powders from being extracted out by the vacuum pump. A heating coil attached with a thermocouple is wrapped up in an insulation box to heat up the vessel. The gas pipes are connected with a hydrogen chamber which provides a sufficient volume of hydrogen for hydriding reaction.

Three high-temperature NiCr-coil type strain gages (H1, H2, and H3) are pasted on the exterior wall surface of the cylindrical vessel. Strain gages H1, H2, and H3 are used to measure the hoop strains at the locations of 7/10, 3/10, and 1/10 height of the vertical vessel from the bottom, respectively. All the reaction steps during cyclic hydriding/dehydriding processes are controlled by a programmable logic controller (PLC). The wall strain and hydrogen pressure data during hydriding/dehydriding reactions are monitored and recorded through a data acquisition system (strainmeter) and a personal computer (PC).

2.2. Material and cyclic hydriding/dehydriding processes

The hydrogen storage alloy, Mg_2Ni, used in the current study was provided by Hsu et al. [36] in a form of ingot made by an innovative mass production technique. The hydriding/dehydriding PCI curves of the given Mg_2Ni alloy at 255–350 °C have been comprehensively studied by Hsu et al. [36]. The hydrogen storage capacity of the given Mg_2Ni alloy measured by a commercial Sieverts-type PCI machine could reach 3.58 wt% [36]. Such a value is very close to the ideal capacity of 3.6 wt% for Mg_2Ni [4]. In order to study the influences of particle size on wall strain variation, the alloy ingot was crushed into powders with two different mesh sizes. One group was sieved with a 100-mesh sieve and the other was sieved with a 200-mesh sieve. The particle size corresponding to 100 and 200 mesh is less than 149 and 74 μm, respectively. Two packing fractions, 50 and 70 vol% (about 13.2 and 18.5 g of Mg_2Ni powders, respectively), were applied to study the effects of packing fraction. Before the cyclic hydriding/dehydriding test, the alloy powders were activated by alternately being evacuated in vacuum at 300 °C for 1 h and then charged with 3-MPa hydrogen at 300 °C for 1 h. After 5 cycles of activation, the cyclic hydriding/dehydriding test started to run in a way that the Mg_2Ni powders were charged with 3-MPa hydrogen at 255 °C for 45 min and then evacuated by a vacuum pump at 255 °C for 60 min. Sizes of the Mg_2Ni powders before the activation process and after the cyclic hydriding/dehydriding test were examined by scanning electron microscopy (SEM).

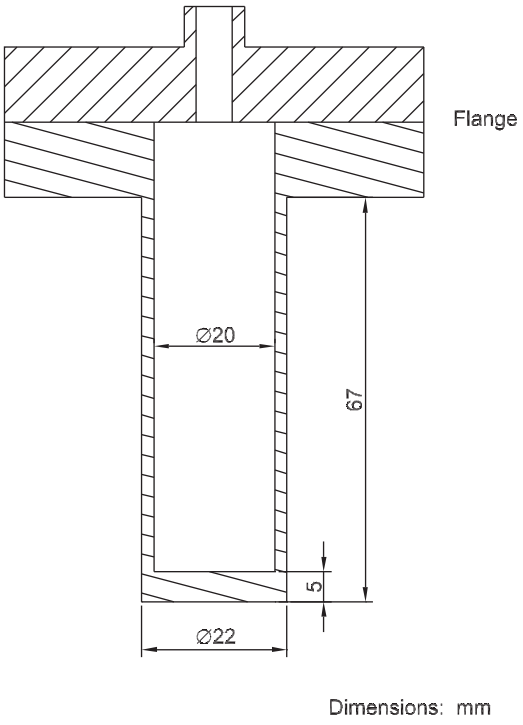

Fig. 1. Geometry of the hydride storage vessel tested.

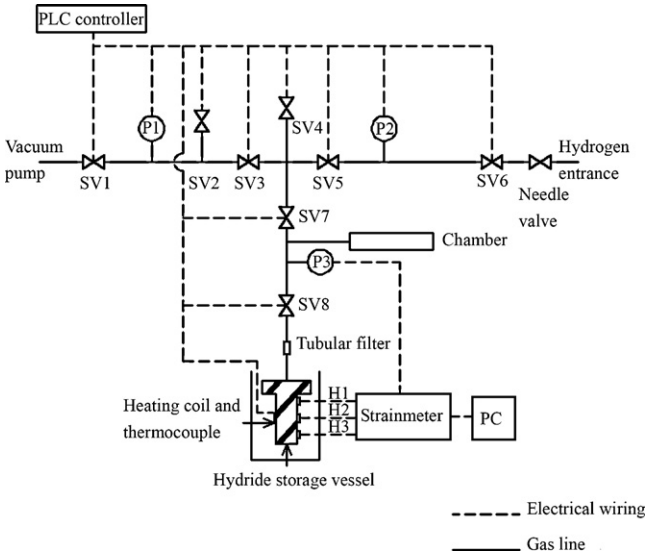

Fig. 2. Schematic diagram of experimental setup.

During the cyclic hydriding/dehydriding reactions, variation of the hoop strain at selected locations (H1–H3) on the vessel surface was measured. Fig. 3 shows the variation of hoop strain at H1, H2, and H3 during the second cycle in a test of 50-vol% packing fraction and an initial powder size of 200 mesh. The strain at H3 (solid line in Fig. 3) is described in details as an example to illustrate the variation of hoop strain. At the beginning of the hydriding/dehydriding cycle, the strain was around zero. When the 3-MPa hydrogen flowed into the reaction vessel, the strain at H3 showed a sudden increase at this moment. As the hydrogen was absorbed rapidly by the

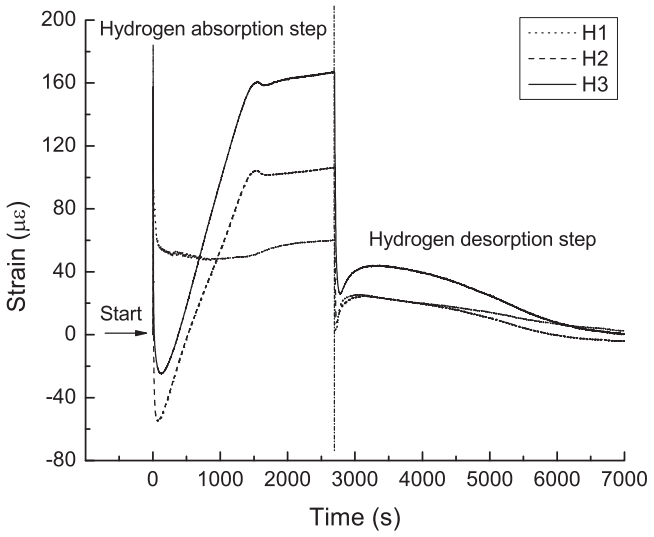

Fig. 3. Variation of hoop strain with time in the second cycle for a packing fraction of 50 vol% of Mg_2Ni powders with a size of 200 mesh.

Mg_2Ni powders, the strain dropped drastically. When the hydrogen atom entered into the lattice of Mg_2Ni, the strain was increased due to a volume expansion of metal hydride formation. At the end of the hydriding step, the reaction between Mg_2Ni and hydrogen tended to become stable. Hence, the strain gradually reached a stable level. At the beginning of the dehydriding step, the redundant hydrogen in the reaction vessel was released to the atmosphere first. Hence, the strain showed a sudden decrease. After that, the hydrogen desorbed by the metal hydrides was continuously extracted to the atmosphere by the vacuum pump. The strain at H3 finally reached a lower level at the end of the dehydriding step as the Mg_2NiH_4 hydrides decomposed hydrogen continuously. Generally, the strain measured include the strains caused by metal hydride expansion and hydrogen pressure. The latter was subtracted from the total strain for analysis purpose. In this regard, only the strains caused by volume expansion of metal hydride formation are presented for each absorption step. In the following discussion, strains at the end of the absorption and desorption steps in each cycle are taken as the data points to show the variation of strain with cycle number for each given test.

3. Results and discussion

3.1. Strain variation at various vessel positions

Fig. 4 shows the hoop strains of various wall positions at the end of the absorption and desorption steps in each cycle for a 50-vol% packing fraction with an initial powder size of 200 mesh.

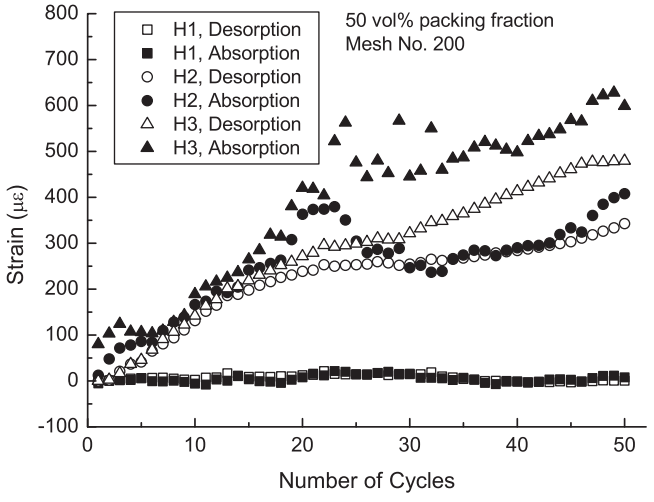

Fig. 4. Variation of hoop strain with cycle number for a packing fraction of 50 vol% of Mg_2Ni powders with an initial size of 200 mesh.

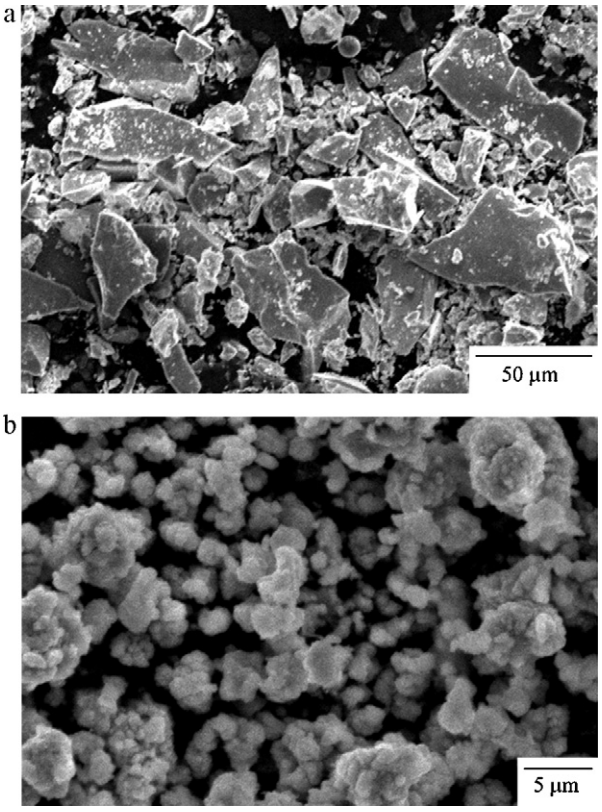

Fig. 5. SEM micrographs of Mg_2Ni powders (200 mesh): (a) before an activation process and (b) after a 50-cycle hydriding/dehydriding test.

The solid and open symbols represent the absorption and desorption steps, respectively. As shown in Fig. 4, the strains of H1 are around zero throughout the test, indicating that hydride-expansion induced wall deformation barely took place at 7/10 height of the vessel. However, the strains of H2 and H3 are greater than zero. The strains of H3 are generally larger than those of H2 and H1 at a given cycle number. For a packing fraction of 50 vol%, the height of the Mg_2Ni powder bed is lower than that of H1. As a result, wall strains at 7/10 height (H1) of the vessel were apparently only affected by the hydrogen gas pressure, while the effect of volume expansion of metal hydride formation was absent at H1. On the other hand, the effect of volume expansion of metal hydride formation was indeed present at positions H2 and H3. The volume expansion and contraction of Mg_2Ni/Mg_2NiH_4 powders during the hydriding/dehydriding reactions could make the alloy powders pulverize. When hydrogen atoms enter into an alloy's lattice, the resultant lattice expansion induces significant microstresses to cause alloy fragmentation [37]. Such alloy pulverization could give rise to particle sedimentation and agglomeration leading to an accumulation of macrostress with progressive cycles on the vessel wall [29]. The pulverized, fine powders could fall down through the gaps between the larger particles under the effect of gravity and generate a densification of powders at lower positions. Therefore, the local powder density is generally increased from the top to the bottom of the vessel. The fine powders at the lower positions could agglomerate at subsequent hydriding/dehydriding cycles. The agglomerated alloy powders are regarded as an important factor in influencing the wall strain of a hydride reaction vessel [26]. Hence, a greater wall strain occurs at a lower position of the vessel. This is the reason why the strains of H3 are generally greater than those of H2 and H1.

Particle sizes of the Mg_2Ni powders observed by SEM before the activation process and after a 50-cycle hydriding/dehydriding test are shown in Fig. 5. Before the activation process, the particles

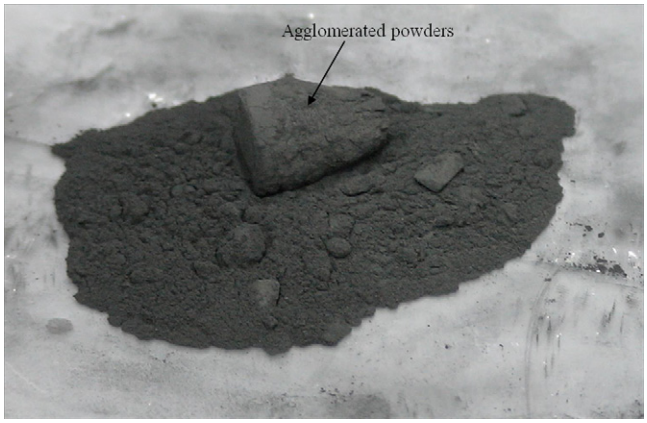

Fig. 6. Photograph of Mg_2Ni powders taken out from an reaction vessel after 50 cycles of hydriding/dehydriding reactions.

showed a wide distribution of size less than 74 μm (Fig. 5(a)). After the 50-cycle test, the particle size was more uniform and reduced to about 1 μm (Fig. 5(b)). Note that the particle shape was initially sharp and irregular and became round after the cyclic test. The pulverization and agglomeration phenomena are evidenced by these SEM micrographs. After the 50-cycle test, the alloy powders taken out from the vessel could be separated into two states, namely loose powders and agglomerated powders, as shown in Fig. 6. Such a photograph indicates the Mg_2Ni powders indeed agglomerated at the bottom of the vessel.

As shown in Fig. 4, the hoop strains at H2 and H3 started to increase with cycle number at the beginning of the cyclic hydriding/dehydriding test. Such a strain accumulation at H2 and H3 was ascribed to the aforementioned pulverization–densification mechanism. At a lower position of the vessel, the local powder density was increased with cycle number due to a continuous fall-down of fine particles through pulverization. Similar strain accumulation phenomena were also observed in other room-temperature hydride storage vessels for $LaNi_5$ and its modified alloys [28,30–32]. Due to a possibly non-uniform distribution and flow of Mg_2Ni powders, the strains of H2 and H3 at the end of each absorption step (solid symbols) had more up-and-down changes throughout the cyclic test. However, for the strains of H2 and H3 at the end of each desorption step (open symbols), a continuously smooth increase with cycle number was observed. Generally speaking, the wall strains of H2 and H3 at the end of the 50th cycle are much larger than those at the first cycle.

3.2. Effects of packing fraction

Fig. 7 shows the variation of hoop strain at H1, H2, and H3 for a 70-vol% packing fraction with an initial powder size of 200 mesh. When the packing fraction was increased to 70 vol%, a small extent of strain accumulation at 7/10 height (H1) was observed. This implies that the top of the Mg_2Ni powder bed was around this height such that the volume expansion of hydride formation induced a certain extent of deformation at H1. In addition, the absorption-step strains at H2 and H3 were very close to each other except at some cycles prior to the 15th cycle, as shown in Fig. 7. In the early cycles, the pulverization-densification mechanism started to take action and increase the local powder density at the bottom of the vessel first such that H3 had a larger expansion strain than did H2. After the 15th cycle, the local powder density at H2 was accumulated to a level similar to that of H3 leading to a comparable extent of wall deformation at both positions until the final stage of test.

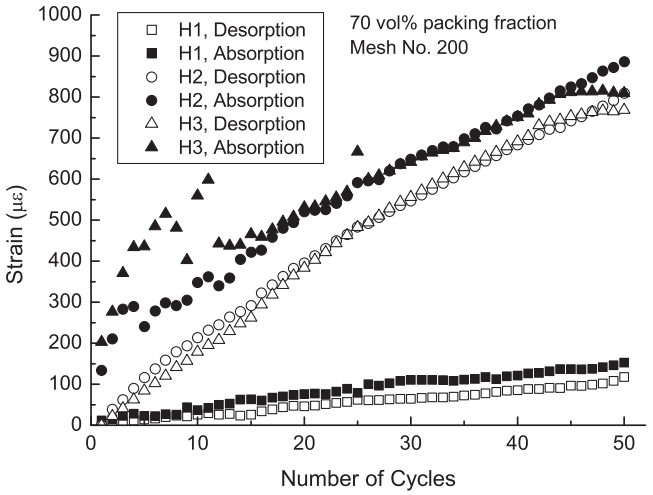

Fig. 7. Variation of hoop strain with cycle number for a packing fraction of 70 vol% of Mg_2Ni powders with an initial size of 200 mesh.

Table 1
Maximum hoop strain during cyclic hydriding/dehydriding processes in a reaction vessel with various combinations of packing fraction and initial particle size of Mg_2Ni powders.

Packing fraction (vol%)	Initial particle size (mesh)	Maximum hoop strain (μm/m)		
		H1	H2	H3
50	200	21	408	628
70	200	157	922	835
50	100	31	667	1344

Comparisons of the maximum wall strain at selected locations are given in Table 1. Apparently, at each given position, a larger packing fraction gave rise to greater wall strains for a given initial particle size of 200 mesh. This is attributed to a greater amount of pulverized, fine powders generated in a larger packing fraction. It would make the alloy powders at lower positions more densified under the effect of gravity. Consequently, the local powder density at H2 and H3 in the case of 70 vol% was significantly greater than that of 50 vol%. Therefore, the maximum hoop strain in a 70-vol% packing fraction is greater than that in a 50-vol% one.

The maximum content of hydrogen absorbed in the reaction vessel at a cycle during the 50-cycle test is listed in Table 2 for each given testing condition. Note the hydrogen storage capacity was calculated as per unit mass of Mg_2Ni. As shown in Table 2, for Mg_2Ni powders with an initial size of 200 mesh, the largest hydrogen storage capacity is 3.23 wt% and 2.95 wt% for the 50-vol% and 70-vol% packing fraction, respectively. The densified, agglomerated stack of fine Mg_2Ni powders formed at the bottom of the vessel is presumably the main reason why the hydrogen storage capacity in the given reaction vessel could not reach the expected hydrogen storage capacity, 3.58 wt% [36]. Note the value of 3.58 wt% was obtained by testing a little amount (2.4 g) of Mg_2Ni alloy in a Sieverts-type

Table 2
Maximum hydrogen storage capacity during cyclic hydriding/dehydriding processes in a reaction vessel with various combinations of packing fraction and initial particle size of Mg_2Ni powders.

Packing fraction (vol%)	Initial particle size (mesh)	Maximum hydrogen storage capacity (wt%)
50	200	3.23
70	200	2.95
50	100	3.25

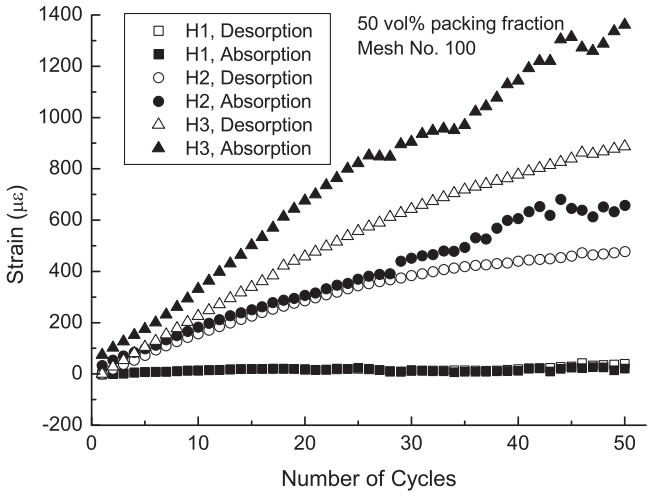

Fig. 8. Variation of hoop strain with cycle number for a packing fraction of 50 vol% of Mg_2Ni powders with an initial size of 100 mesh.

PCI machine and no agglomeration of alloy powders was observed [36]. Dehouche et al. [12] observed that a compaction of alloy powders would enlarge the pressure hysteresis and increase the plateau slope in PCI curves. As the gaps between the alloy powders become smaller in the densified regions, the agglomerated stack would somehow retard the hydrogen delivery. Moreover, the available, active surface area of Mg_2Ni powders to react with hydrogen also becomes smaller in the agglomerated regions, as compared to loose powders. Hence, the hydrogen storage capacity in the given reaction vessel is lower than the expected value of 3.58 wt%. Similarly, the lower hydrogen storage capacity of the 70-vol% packing fraction given in Table 2, compared to the 50-vol% one, could be attributed to a greater extent of agglomeration of Mg_2Ni powders.

3.3. *Effects of initial particle size*

Variation of the hoop strain at various positions with cycle number for a 50-vol% packing fraction with an initial powder size of 100 mesh is shown in Fig. 8. Note that the particle size of 100 mesh is larger than that of 200 mesh. In comparison of Figs. 4 and 8, a greater extent of difference in the strain between H2 and H3 is found for the case of 100 mesh. This is attributable to the size of gaps between Mg_2Ni powders in the vessel. A larger, initial particle size would generate larger gaps such that the pulverized, fine powders could fall downward more easily through these larger gaps. Consequently, the local powder density at a lower position such as H3 is expected to be greater in a larger, initial particle size. Therefore, the extent of difference in the local powder density between H3 and H2 was enlarged when the initial particle size of Mg_2Ni powders was increased from 200 mesh to 100 mesh. Table 1 also gives comparisons of the maximum wall strains between these two different initial particle sizes. Apparently, at a given position on the vessel wall, a larger, initial particle size gave rise to greater hoop strains. In addition, such an increase in the magnitude of wall deformation caused by a larger, initial size is dependent on wall position. The extent of difference in the absorption-step strain between the given two initial particle sizes at H3 is much larger than that at H2 and H1.

As shown in Table 2, the largest hydrogen storage capacity in a reaction vessel with a 50-vol% packing fraction is 3.23 wt% for 200 mesh and 3.25 wt% for 100 mesh. Apparently, for given a packing fraction of 50 vol%, the hydrogen storage capacity of the reaction vessel is slightly greater for a larger, initial particle size. In general, a smaller, initial particle size of alloy powder is expected to enhance the reaction with hydrogen and increase the hydrogen storage capacity, due to a higher surface/volume ratio. However, the results in Table 2 does not show such a trend. As reported previously, an agglomeration phenomenon tended to occur more easily for a smaller, initial particle size of hydrogen absorbing alloy powders [33]. The volume expansion of alloy powders in the agglomerated stack during hydriding processes could compress the limited amount of gaps between fine particles and inhibit a uniform hydrogen distribution. A larger, initial powder size presumably provides more larger gaps for hydrogen flow paths. Hence, the hydrogen storage capacity of the Mg_2Ni reaction vessel packed with an initial particle size of 100 mesh is slightly greater than that of 200 mesh.

4. Conclusions

(1) Wall strain accumulation phenomena were present in a vertical high-temperature Mg_2Ni storage vessel. A pulverization-densification mechanism was responsible for such strain accumulation behavior.
(2) For a given position on the vessel wall, a larger packing fraction of Mg_2Ni powders induced a greater extent of deformation during cyclic hydriding/dehydriding reactions.
(3) Agglomerated Mg_2Ni powders were found at the bottom of the reaction vessel after cyclic hydriding/dehydriding tests. The agglomeration could degrade the hydrogen storage capacity of a hydride reaction vessel.
(4) A larger, initial particle size induced a greater hoop strain in the vessel wall, due to a greater local powder density at lower positions of the vessel.
(5) Regardless of the initial size of Mg_2Ni powders, the alloy particles were reduced to a size of about 1 μm after a 50-cycle hydriding/dehydriding test.

Acknowledgements

This work was supported by the National Science Council (Taiwan) under Contract Nos. NSC 98-2221-E-008-003 and NSC 99-2221-E-008-014.

References

[1] B. Sakintuna, F. Lamari-Darkrim, M. Hirscher, Int. J. Hydrogen Energy 32 (2007) 1121–1140.
[2] I.P. Jain, C. Lal, A. Jain, Int. J. Hydrogen Energy 35 (2010) 5133–5144.
[3] P. Selvam, B. Viswanathan, C.S. Swamy, V. Srinivasan, Int. J. Hydrogen Energy 11 (1986) 169–192.
[4] J.J. Reilly, R.H. Wiswall, Inorg. Chem. 7 (1968) 2254–2256.
[5] T. Malinova, Z.X. Guo, Mater. Sci. Eng. A 365 (2004) 219–227.
[6] J. Cermak, L. Kral, Int. J. Hydrogen Energy 33 (2008) 7464–7470.
[7] Y.H. Zhang, B.W. Li, H.P. Ren, F. Hu, G.F. Zhang, S.H. Guo, J. Alloys Compd. 509 (2011) 5604–5610.
[8] Y.H. Zhang, B.W. Li, H.P. Ren, X.X. Ding, X.G. Liu, L.L. Chen, J. Alloys Compd. 509 (2011) 2808–2814.
[9] Y.H. Zhang, F. Hu, Z.G. Ki, K. Lu, S.H. Guo, X.L. Wang, J. Alloys Compd. 509 (2011) 294–300.
[10] H.W. Wang, S.D. Chyou, S.H. Wang, P.K. Chiu, C.C. Yen, B.Y. Chen, M.W. Yang, H.C. Tien, N.N. Huang, J. Alloys Compd. 491 (2010) 623–626.
[11] D. Sun, H. Enoki, F. Gingl, E. Akiba, J. Alloys Compd. 285 (1999) 279–283.
[12] Z. Dehouche, R. Djaozandry, J. Goyette, T.K. Bose, J. Alloys Compd. 288 (1999) 269–276.
[13] F.S. Yang, G.X. Wang, Z.X. Zhang, X.Y. Meng, V. Rudolph, Int. J. Hydrogen Energy 35 (2010) 3832–3840.
[14] J. Cieslik, P. Kula, R. Sato, J. Alloys Compd. 509 (2011) 3972–3977.
[15] A.T. Wijayanta, K. Nakaso, T. Aoki, Y. Kitazato, J. Fukai, Int. J. Hydrogen Energy 36 (2011) 3529–3536.
[16] J.H. Ye, L.J. Jiang, Z.N. Li, X.P. Liu, S.M. Wang, X.Y. Li, Int. J. Hydrogen Energy 35 (2010) 8216–8224.
[17] A. Chaise, P. de Rango, Ph. Marty, D. Fruchart, Int. J. Hydrogen Energy 35 (2010) 6311–6322.
[18] M. Melnichuk, N. Silin, G. Andreasen, H.L. Corso, A. Visintin, H.A. Peretti, Int. J. Hydrogen Energy 35 (2010) 5855–5859.
[19] C.A. Chung, C.J. Ho, Int. J. Hydrogen Energy 34 (2009) 4351–4364.
[20] C.A. Chung, C.S. Lin, Int. J. Hydrogen Energy 34 (2009) 9409–9423.

[21] H. Dhaou, A. Souahlia, S. Mellouli, F. Askri, A. Jemni, S. Ben Nasrallah, Int. J. Hydrogen Energy 35 (2010) 1674–1680.
[22] S. Mellouli, F. Askri, H. Dhaou, A. Jemni, S. Ben Nasrallah, Int. J. Hydrogen Energy 35 (2010) 1693–1705.
[23] A. Souahlia, H. Dhaou, F. Askri, S. Mellouli, A. Jemni, S. Ben Nasrallah, Int. J. Hydrogen Energy 36 (2011) 4952–4957.
[24] M.L. Tsai, T.S. Yang, Int. J. Hydrogen Energy 35 (2010) 11052–11063.
[25] G. Capurso, F. Agresti, S. Lo Russo, A. Maddalena, G. Principi, A. Cavallari, C. Guardamagna, J. Alloys Compd., (2010), doi:10.1016/j.jallcom.2010.11.104, in press.
[26] Q.D. Wang, J. Wu, C.P. Chen, Z.P. Li, J. Less-Common Met. 131 (1987) 399–407.
[27] S.T. McKillip, C.E. Bannister, E.A. Clark, Fusion Technol. 21 (1992) 1011–1016.
[28] K. Nasako, Y. Ito, N. Hiro, M. Osumi, J. Alloys Compd. 264 (1998) 271–276.
[29] K. Nasako, Y. Ito, N. Hiro, M. Osumi, Int. J. Hydrogen Energy 23 (1998) 921–929.
[30] B.Y. Ao, S.X. Chen, G.Q. Jiang, J. Alloys Compd. 390 (2005) 122–126.
[31] F. Qin, L.H. Guo, J.P. Chen, Z.J. Chen, Int. J. Hydrogen Energy 33 (2008) 709–717.
[32] F. Qin, J.P. Chen, Z.J. Chen, Mater. Des. 29 (2008) 1926–1933.
[33] T. Saito, K. Suwa, T. Kawamura, J. Alloys Compd. 253/254 (1997) 682–685.
[34] S. Ono, Y. Ishido, K. Imanari, T. Tabata, J. Less-Common Met. 88 (1982) 57–61.
[35] S. Enache, W. Lohstroh, R. Griessen, Phys. Rev. B 69 (2004), 115326-1–115326-12.
[36] C.W. Hsu, S.L. Lee, R.R. Jeng, J.C. Lin, Int. J. Hydrogen Energy 32 (2007) 4907–4911.
[37] R.A. Oreani, Fusion Technol. 26 (1994) 235–266.